The Astrophysical Journal Letters, 1003:L14 (7pp), 2026 May 20 https://doi.org/10.3847/2041-8213/ae64e1

The Pristine He II Emitter near GN-z11: Constraining the Mass Distribution of the First Stars

Elka Rusta[1,2], Stefania Salvadori[1,2], Roberto Maiolino[3,4,5], Viola Gelli[6,7], Ioanna Koutsouridou[1], Stefano Carniani[8], Hannah Übler[9], Alessandro Marconi[1,2], and Daniel Schaerer[10]

[1] Dipartimento di Fisica e Astronomia, Università degli Studi di Firenze, Largo E. Fermi 1, 50125, Firenze, Italy; elka.rusta@unifi.it
[2] INAF/Osservatorio Astrofisico di Arcetri, Largo E. Fermi 5, 50125, Firenze, Italy
[3] Kavli Institute for Cosmology, University of Cambridge, Madingley Road, Cambridge CB3 0HA, UK
[4] Cavendish Laboratory, University of Cambridge, 19 JJ Thomson Avenue, Cambridge CB3 0HE, UK
[5] Department of Physics and Astronomy, University College London, Gower Street, London WC1E 6BT, UK
[6] Cosmic Dawn Center (DAWN), Denmark
[7] Niels Bohr Institute, University of Copenhagen, Jagtvej 128, 2200 Copenhagen N, Denmark
[8] Scuola Normale Superiore, Piazza dei Cavalieri 7, 56126 Pisa, Italy
[9] Max-Planck-Institut für extraterrestrische Physik, Gießenbachstraße 1, 85748 Garching, Germany
[10] Department of Astronomy, University of Geneva, Chemin Pegasi 51, 1290 Versoix, Switzerland
Received 2026 March 19; revised 2026 April 24; accepted 2026 April 25; published 2026 May 18

Abstract

The properties of the first metal-free stars remain largely unknown, and so far, the only data-driven constraints on their initial mass function (IMF) come from near-field cosmology. Here, we interpret new observations of the C1 and C2 components of Hebe, the He II emitter near the galaxy GN-z11. Using a locally calibrated model, we robustly confirm the pristine (Population III, Pop III) nature of both components, showing that the measured upper limits on metal lines can only be reproduced by galaxies with >50% of their stellar mass in Pop III stars. We find that C1 is consistent with a purely Pop III system and adopt a simple parametric approach to infer the implications for the Pop III IMF and stellar mass. The observed He II/Hγ ratio excludes steep IMFs, favoring top-heavy distributions, especially for young stellar ages ($\leqslant$1 Myr). Combined with the He II luminosity, this implies a total Pop III stellar mass of $2 \cdot 10^4 < M_\star/M_\odot < 6 \cdot 10^5$. While degeneracies between IMF, stellar mass, and age remain, adopting the lower stellar masses predicted by simulations ($M_\star < 10^5\,M_\odot$) strengthens the preference for top-heavy IMFs. Combining these results with near-field constraints, which instead exclude the flattest IMFs, we define a data-driven range of viable Pop III IMFs, linking characteristic mass and slope. This work demonstrates that direct observations of high-z Pop III systems can place independent constraints on the IMF of the first stars, opening a new window on their formation and properties.

Unified Astronomy Thesaurus concepts: Population III stars (1285); High-redshift galaxies (734); James Webb Space Telescope (2291)

1. Introduction

Uncovering the nature of the first stars is one of the key goals of present-day cosmology and of the JWST mission. Also known as Population III (hereafter, Pop III) stars, they produce the first ionizing photons, the first elements heavier than helium, and the first stellar black holes (BHs), thus profoundly affecting the galaxy formation process (e.g., V. Bromm 2013). In particular, the initial mass function (IMF) of Pop III stars, i.e., the Pop III IMF, regulates the number and type of photons and chemical elements, and BHs produced in the early Universe, thereby determining how reionization and metal enrichment began, while their role in supermassive BH seeding remains uncertain.

However, the Pop III IMF remains largely unknown. Cosmological simulations of the first star-forming systems predict different typical masses for Pop III stars (e.g., R. S. Klessen & S. C. O. Glover 2023). Thus, so far, the only constraints on the Pop III IMF come from near-field cosmology. The nondetection of long-lived metal-free stars in ultrafaint dwarf galaxies sets a lower limit on the peak of the Pop III IMF, $M_{\rm ch} > 1 M_\odot$ (M. Rossi et al. 2021). In the Galactic halo, the absence of stars showing the key chemical signatures of pair instability supernovae (PISNe; S. Salvadori et al. 2019) excludes the flattest Pop III IMFs (I. Koutsouridou et al. 2024).

Ultimately, Pop III stars were likely more massive than subsequent generations of metal-enriched (Pop II) stars. However, a wide variety of plausible Pop III IMFs remains: the peak can range from one to hundreds of solar masses, and the slope can be either flatter or steeper than Salpeter, although not completely flat. Can we use JWST observations of high-z galaxies to further constrain the Pop III IMF?

The highly ionizing emission of Pop III stars produces characteristic helium II (He II) recombination lines, like He II λ1640 (e.g., J. Tumlinson & J. M. Shull 2000; S. P. Oh et al. 2001; A. K. Inoue 2011; E. Zackrisson et al. 2011; K. Nakajima & R. Maiolino 2022; M. Lecroq et al. 2025). Hence, we expect a strong He II in the emission of systems hosting Pop III stars, combined with signatures of either metal-free or metal-poor gas enriched by the first Pop III supernovae (SNe).

Despite extensive searches, only a handful of Pop III candidates have been identified with JWST so far. All but one are at least *very metal-poor systems* at $z < 7$ (e.g., E. Vanzella et al. 2023; K. Nakajima et al. 2025), with some potentially being metal free (T. Morishita et al. 2025; E. Vanzella et al. 2026), yet they currently lack the He II detection expected for Pop III stars. Only the $z = 10.6$ companion of GN-z11 matches the expected properties of a pure Pop III galaxy, showing a combination of both a strong He II emission, with EW(He II λ1640) > 20 Å, and the absence of detectable metal lines (R. Maiolino et al. 2024).

Deeper JWST observations reported in two companion papers have now revealed that this system, which we will dub *Hebe*,[11] consists of two components, C1 and C2, both showing He II emission (R. Maiolino et al. 2026), along with tight upper limits on rest-frame UV and optical metal lines, and a Hγ detection in C2 (H. Übler et al. 2026).

In this Letter, we use the model presented in E. Rusta et al. (2025) to interpret the new observations of Hebe and assess their implications, addressing urgent questions: Is the companion of GN-z11 a truly pristine Pop III system, or is it also consistent with a very metal-poor Pop II (or hybrid) galaxy? Can we use the observed spectral features of its components to further constrain the Pop III IMF?

2. Methods: Recap of the Model

We adopt the model of E. Rusta et al. (2025), which combines the locally calibrated galaxy formation code NEFERTITI, stellar population synthesis libraries, and the publicly available code CLOUDY. With this modeling framework, we can self-consistently trace the chemical enrichment and spectral evolution of Pop III galaxies and thus combine constraints on the Pop III IMF from both near- and far-field cosmology.

As defined in E. Rusta et al. (2025), we subdivide Pop III galaxies into the following groups: *pristine*—only Pop III stars and metal-free gas; *self-polluted*—only Pop III stars and Pop III-enriched gas; and *Pop III–rich/mid/poor hybrids*—mixture of Pop III and Pop II stars, respectively, with >50%, 25%–50%, and <25% of the total stellar mass in metal-free stars.

2.1. The NEFERTITI Semianalytical Model

We employ the NEFERTITI model coupled with a dark matter cosmological simulation of a Milky Way analog (see I. Koutsouridou et al. 2023) to simulate Pop III galaxies at high z (E. Rusta et al. 2024). Given its calibration with near-field cosmology data (I. Koutsouridou et al. 2023, 2024, 2025), the model is particularly suitable for studying the properties of the first stars. NEFERTITI follows the formation and evolution of individual stars, starting from pristine gas, and self-consistently traces the chemical enrichment of the gas. Stars are formed following a Larson-type IMF (R. B. Larson 1998):

$$\phi(m_\star) = \frac{dN}{dm_\star} \propto m_\star^{-x} \exp\left(-\frac{M_{\rm ch}}{m_\star}\right), \quad (1)$$

where x represents the slope of the IMF and $M_{\rm ch}$ the characteristic mass, i.e., the IMF peak. For Pop III stars, we assume a mass range $m_\star = [0.8\text{–}1000] M_\odot$, a fiducial value of $x = 2.35$, and explore $M_{\rm ch} = [1, 10, 70] M_\odot$ (see I. Koutsouridou et al. 2023, 2024). For Pop II stars, a mass range $m_\star = [0.08\text{–}100] M_\odot$, $x = 2.35$, and $M_{\rm ch} = 0.35 M_\odot$.

For this project, we analyze a set of 250 Pop III galaxies and 205 metal-poor Pop II galaxies (with $\log {\rm O/H} + 12 < 7.5$) simulated with NEFERTITI at $z = 10.6$, the observed redshift of Hebe.

2.2. The Spectral Synthesis and CLOUDY Models

We produce the synthetic spectra of our set of NEFERTITI galaxies by constructing the stellar continuum and then running photoionization models with CLOUDY (C23 release; G. J. Ferland et al. 1998; M. Chatzikos et al. 2023) to obtain the nebular emission. For the stellar emission, we use individual stellar spectra and evolutionary tracks from D. Schaerer (2002) for Pop III stars, both to account for the incomplete IMF sampling and to freely vary the IMF shape and range, and IMF-integrated spectra from D. Schaerer (2003) and E. Zackrisson et al. (2011) for Pop II stars. We then input both the total stellar continuum and the chemical composition of the gas into the CLOUDY code to self-consistently trace the metal enrichment in the transition from Pop III to hybrid galaxies.

We adopt the same CLOUDY modeling assumptions as in E. Rusta et al. (2025), with gas density $n_{\rm H} = 10^3$ cm^{-3} and ionization parameters $\log U = [0, -0.5, -1, -2]$. We also run a high-density case with $n_{\rm H} = 10^6$ cm^{-3} and $\log U = -2$. Considering the different Pop III galaxy stages and parameters explored, we ultimately obtain a set of 5000 photoionization models for Pop III galaxies and 820 for metal-poor Pop II galaxies.

3. The Pristine Nature of Hebe

We first explore the nature of Hebe by using our Pop III models to interpret the observed line ratios reported by R. Maiolino et al. (2026) for the individual C1 and C2 components. Figure 1 compares the measured 3σ upper limits on the C IV, C III], and O III] emission lines[12] relative to He II, with the predictions of our model for Pop III galaxies in different evolutionary stages, and for metal-poor Pop II galaxies.

We clearly see that even upper limits on these metal species are highly informative when compared with model predictions. Indeed, we find that both C1 and C2 are not consistent with either Pop II galaxies or Pop III-poor hybrids and are instead fully consistent with being *at least* Pop III–rich galaxies, i.e., with >50% of their stellar mass in metal-free stars, and with having $\log {\rm O/H} < 7.4$. Moreover, they are potentially consistent with pristine (or self-polluted) Pop III galaxies, hence composed exclusively of Pop III stars and containing metal-free (or Pop III-enriched) gas, with C1 appearing more pristine than C2. This Pop III scenario is further supported by the two companion papers (R. Maiolino et al. 2026; H. Übler et al. 2026), showing that this is the most plausible among others (e.g., direct collapse BHs).

Based on this result, we now focus on models with >50% of stellar mass in Pop III stars and move on to explore the impact of the Pop III IMF on the He II emission. In Figure 2, we show the EW(He II) versus the He II/Hγ ratio predicted for pristine Pop III, self-polluted Pop III, and Pop III–rich hybrids, together with Hebe data. We note that with increasing characteristic mass, i.e., for progressively top-heavier Pop III IMFs, the distribution of Pop III galaxies peaks at higher EW(He II) and He II/Hγ values, and the peak also becomes more pronounced. Indeed, for top-heavy Pop III IMFs, there is a higher probability of forming very massive stars, which have the strongest He II emission. More specifically, for increasing

[11] Helium balmer emitter. In ancient Greek mythology, Hebe (LGRLGRH$H\beta\eta$) is the goddess of youth, daughter of Zeus and Hera.

[12] Notation: C IV for C IV $\lambda\lambda$1548, 1551; C III] for C III]λ1907 + λ1909; O III] for O III] $\lambda\lambda$1661, 1666; and He II for He II λ1640.

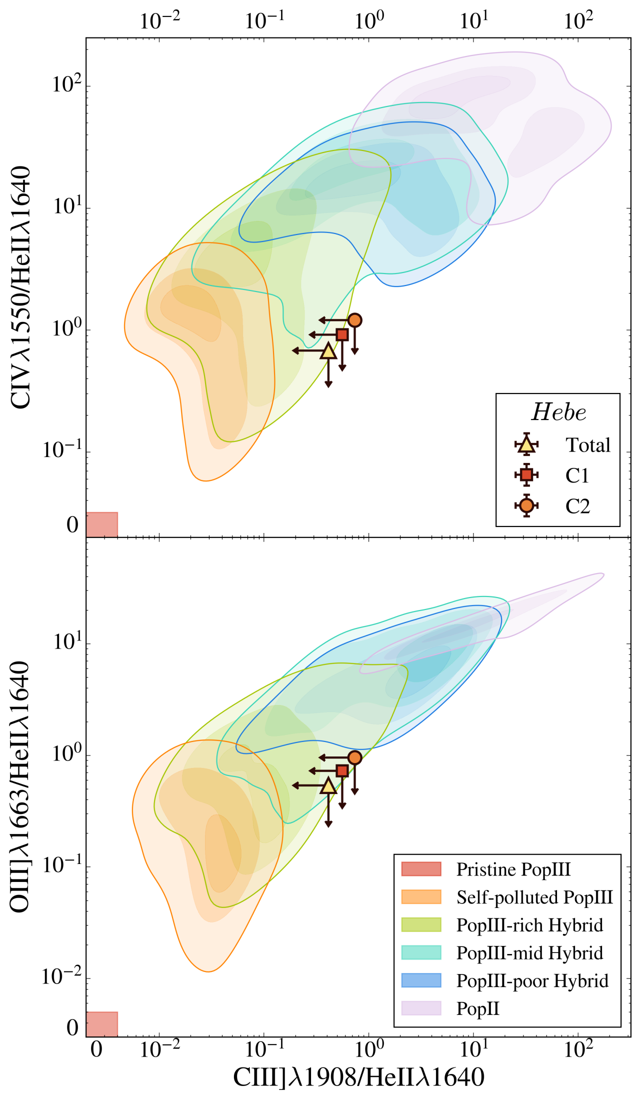

Figure 1. Density distributions of our NEFERTITI models at $z = 10.6$ for Pop III galaxies at different evolutionary stages (red: pristine; orange: self-polluted; green: Pop III–rich hybrids; cyan: Pop III-mid hybrids; blue: Pop III-poor hybrids); and for metal-poor Pop II galaxies (purple). The solid contours include 68% of the galaxy population, for $\log U = [-2, -1, -0.5, 0]$ altogether. The error bars are the 3σ observational upper limits presented in R. Maiolino et al. (2026).

M_{ch}, we find that the probability P(EW(He II) > 50 Å) goes from 26% to 40% and reaches 69% for the most top-heavy IMF.

Interestingly, C1 is fully consistent with the peaks of the distribution of our Pop III galaxy models for all three IMFs explored and could potentially lie on the EW(He II) versus He II/Hγ relation predicted for Pop III stars.

Conversely, C2 shows a lower He II/Hγ ratio while maintaining the high EW(He II) characteristic of Pop III stars. However, unlike the diagnostics shown in Figure 1, the He II/Hγ ratio may be significantly affected by dust as it combines UV and optical lines. The presence of dust would decrease the He II/Hγ without affecting EW(He II), implying that C2 could be a self-polluted or hybrid Pop III system enriched by recent Pop III SNe. As discussed in R. Maiolino et al. (2026), an extinction of only $A_V \sim 0.25$ would be sufficient to match our Pop III predictions when adopting the extinction curve from F. Sun et al. (2026). Using instead the flatter relation derived by V. Markov et al. (2025), we estimate $A_V \sim 1.4$. This implies larger dust masses $\leqslant 50\,M_\odot$ for a very compact configuration, which can, however, be provided by a few PISNe, each one producing $>10\,M_\odot$ of dust (T. Nozawa et al. 2003; R. Schneider et al. 2004). An alternative scenario involves very high gas densities, as shown by the high-density ($n_H = 10^6$ cm^{-3}) models reported in Figure 2 with lighter colors. For Pop III stars, the continuum at the wavelength of He II is dominated by two-photon emission (e.g., A. Raiter et al. 2010), which is heavily suppressed at $n_H \geqslant 10^5$ cm^{-3}. For this reason, the high-density models have much higher EW(He II) while maintaining a similar He II/Hγ ratio. This would also suggest that C2 is a hybrid galaxy, consistent with the interpretation of H. Übler et al. (2026).

Given these findings, we will now focus on the interpretation of the C1 component of Hebe as an archetypal pure Pop III system.

4. Exploring Pop III IMF and Stellar Mass

The system Hebe lies in a dense and peculiar environment, being the companion of GN-z11, one of the most massive galaxies observed at high redshift. In contrast, our data-calibrated cosmological model NEFERTITI focuses on the assembly of the Milky Way, which corresponds to a smaller fluctuation of the density field. As a result, at $z = 10.6$, the model predicts Pop III galaxies that are less luminous than the GN-z11 companion, with total stellar masses $M_\star \leqslant 4 \cdot 10^3\,M_\odot$ (see Figure 6 in the Appendix). While this does not affect comparisons of emission line ratios or equivalent widths, which are independent of the total stellar mass, it prevents a direct interpretation of the observed line luminosities.

Here, we develop a simple parametric approach to use the observed He II/Hγ ratio and the He II luminosity, $L_{\rm He\,II} = (5.1 \pm 0.9) \cdot 10^{40}$ erg s^{-1}, of C1 to constrain the Pop III IMF and stellar mass. To this end, we compute the synthetic emission from a single Pop III star formation episode at different ages (1 Myr steps), using the same CLOUDY parameters as in Section 2, and with a fully sampled IMF. This assumption is discussed in the Appendix, where Figure 6 shows how the predicted He II luminosity varies with the total mass of Pop III stars formed, $M_\star$, when the fiducial IMF is randomly or fully sampled. To explore the IMF widely, we vary both the peak M_{ch} in the range [1–300] $M_\odot$ and the slope x between 0 (flat) and 4.35 (steep), keeping a fixed mass range of [0.8–1000]$M_\odot$ (see Equation (1)). The validity of this assumption is discussed at the end of the section. We focus on the emission at 1 Myr and 2 Myr after the star formation episode to provide a reasonable range of results. Indeed, immediately after the birth of Pop III stars (0 Myr), the emission takes intermediate values between those considered here, while by 3 Myr, the He II emission is already too faint due to the death of the most massive stars (D. Schaerer 2002).

As seen also in Figure 2, He II/Hγ depends on the Pop III IMF, but not on the total stellar mass formed, $M_\star$, since it is an emission line ratio. In contrast, line luminosities scale strongly with $M_\star$ (see Figure 6 for a fixed IMF), motivating our parametric study, shown in Figure 3. We thus use He II/Hγ to exclude Pop III IMFs, which are not consistent with the observed ratio, independently of $M_\star$ (left panels). For the remaining Pop III IMFs, we then determine the stellar mass required to obtain the observed $L_{\rm He\,II}$ (right panels). In both

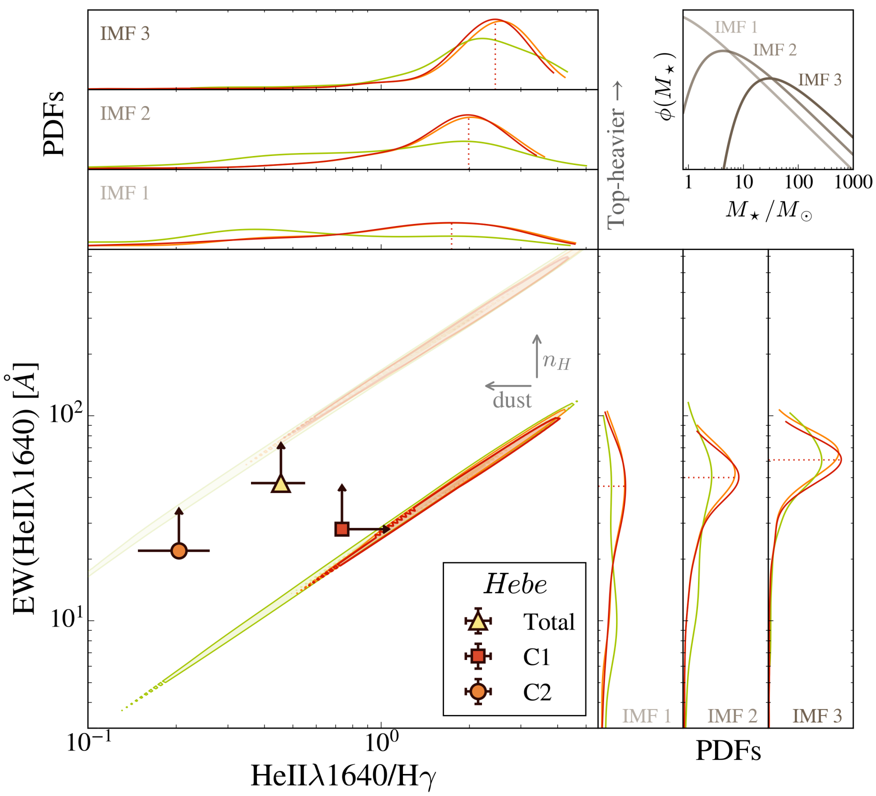

Figure 2. EW(He II) versus He II/Hγ for the subsample of NEFERTITI galaxies at $z = 10.6$ that match the upper limits on metal emission lines (Figure 1), shown for three Pop III IMFs as indicated in the top-right scheme (Salpeter slope $x = 2.35$, peak mass $M_{ch} = [1, 10, 70]M_\odot$). For each IMF, we show the PDFs of different Pop III galaxy types: pristine (red), self-polluted (orange), and Pop III–rich hybrids (green). Arrows indicate how dust and/or higher gas densities would modify the observed properties of these Pop III galaxies. We also report in lighter colors the high-density models (i.e., $n_H = 10^6$ cm^{-3}). The error bars are the 3σ data from R. Maiolino et al. (2026) and H. Übler et al. (2026).

cases, we show the results of our parametric study for ages 1 Myr (first row) and 2 Myr (second row).

At the age of 2 Myr, we obtain the highest He II luminosities and He II/Hγ ratios, corresponding to the peak of the He II emission produced by the most massive Pop III stars in the adopted stellar population libraries (D. Schaerer 2002). The left panels of Figure 3 show the regions excluded by the lower limits on the observed He II/Hγ of C1 at different confidence levels. Steep Pop III IMFs with low M_{ch} fail to reproduce the high observed value (He II/Hγ > 0.7 at 3σ) and can therefore be ruled out. However, the minimum M_{ch} implied by the 3σ, 2σ, and 1σ limits depends on both the assumed stellar age and IMF slope. For example, for an age of 1 Myr and a Salpeter slope ($x = 2.35$), the 3σ limit requires $M_{ch} \gtrsim 75\, M_\odot$, favoring relatively top-heavy Pop III IMFs.

The right panels show the stellar masses required for each Pop III IMF to reproduce the He II luminosity of C1, with the IMFs excluded by the He II/H_γ constraints (left panels) indicated in red. We find that models matching both the observed He II/H_γ ratio and the He II luminosity predict total stellar masses of $10^{4.25-5.8}\, M_\odot$, with the exact value depending on the stellar population age and the assumed IMF. The minimum mass is obtained for an age of 2 Myr and a flat Pop III IMF. Conversely, steeper Pop III IMFs require either a larger M_{ch} or a higher stellar mass to reproduce the high observed $L_{\rm He\,II}$. We stress that the Pop III IMFs implying the largest stellar masses are already excluded (see left panels of Figure 3), as they fail to reproduce the observed He II/H_γ ratio.

Additionally, we investigate the impact of varying the Pop III IMF mass range to validate our assumption of [0.8–1000]$M_\odot$. While the minimum mass has a negligible effect on our results, the maximum mass strongly affects our predictions. For this reason, we explore $M_{max} = [100 - 1000]M_\odot$ for a fixed Salpeter slope. In Figure 4, we report the M_{max}, which can be excluded, as a function of M_{ch}, based on the He II/Hγ observed in the C1 component of Hebe. These are the most conservative constraints, taken at the age of the peak He II emission. We find that a standard $M_{max} = 100M_\odot$ can be excluded at 2σ confidence level if $M_{ch} \in (50–100)M_\odot$ and at 3σ for $M_{ch} \in (1–50)M_\odot$. For fixed $M_{ch} = 10M_\odot$, the maximum mass must be at least $150M_\odot$ (3σ), $200M_\odot$ (2σ), or $460M_\odot$ (1σ). Notably, we also find that for a flat Pop III IMF, $M_{max} > 200M_\odot$ at 1σ. Hence, our assumption of a mass range up to $1000M_\odot$ is in agreement with Hebe for all the M_{ch} explored.

Ultimately, our analysis of the C1 component of Hebe favors a top-heavy Pop III IMF.

5. Discussion and Conclusions

The first confirmation of a pristine He II emitter at $z = 10.6$, i.e., Hebe, showcases the enormous advances made by JWST in the quest for Pop III stars. Direct detections of high-z galaxies hosting Pop III stars are crucial to complement our limited knowledge of the first stars' properties, currently based on near-field cosmology studies. In this Letter, we use a locally calibrated model to robustly confirm the Pop III nature of Hebe and explore its implications by combining near- and far-field approaches.

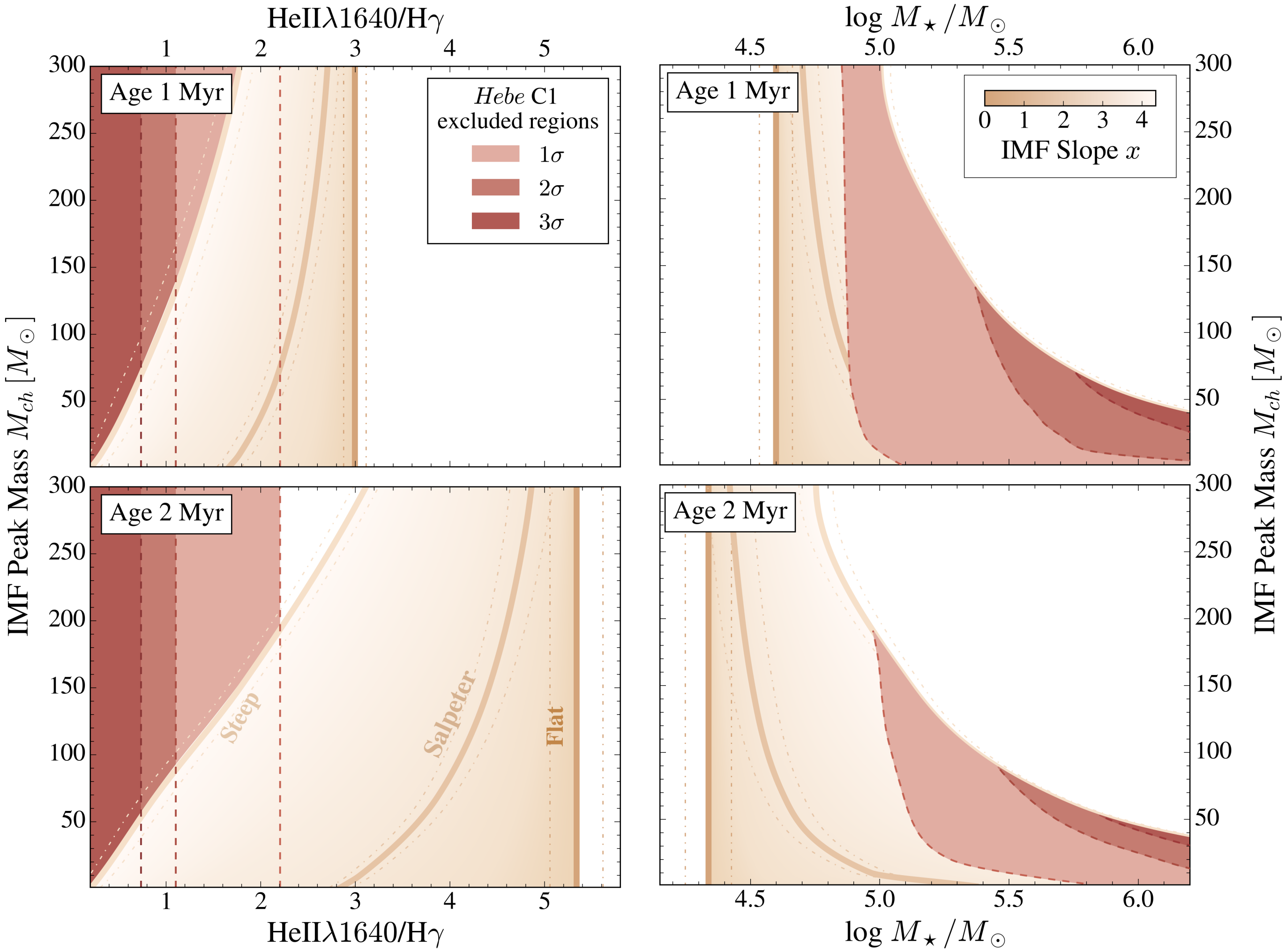

Figure 3. Left: predicted He II/Hγ emission from Pop III stars for ages 1 Myr (top) and 2 Myr (bottom), for different M_{ch} and IMF slope (beige regions). The red areas indicate the 3σ, 2σ, and 1σ lower limits measured by R. Maiolino et al. (2026) in the C1 component of Hebe. Right: mass of Pop III stars required to reproduce the observed $L_{\rm He\,II}$ value of C1 for ages 1 Myr (top) and 2 Myr (bottom), using different M_{ch} and IMF slopes. Red areas mark IMFs excluded by the He II/Hγ constraints (left panels). In *both the left and right panels*, the beige scale shows different Pop III IMF slopes (see legend in the top-right panel) with solid lines highlighting the flat ($x = 0$), Salpeter, and steep ($x = 4.35$) slopes. For these three examples, the dotted lines represent the scatter due to $\log U = [0, -2]$, and the error of the measured $L_{\rm He\,II}$ value.

Initially, we investigate the upper limits on UV metal lines, comparing observations with Pop III and Pop II galaxy predictions obtained from the NEFERTITI model. Adopting a cosmological model that reproduces present-day observations of ancient metal-poor stars allows us to obtain reliable predictions for the early chemical enrichment. For both the C1 and C2 components in Hebe, models with <50% Pop III stellar mass fail to reproduce the observations. We find that C1 is fully consistent with a pure Pop III system, composed exclusively of Pop III stars and surrounded by either pristine gas or gas self-enriched by Pop III SNe (see Section 2). This makes C1 the most compelling candidate for a genuinely pristine stellar system identified to date.

Treating C1 as an archetypal pristine Pop III system, we explore the Pop III IMF to constrain its shape and characteristic mass, using a Larson-type IMF with $m_\star = [0.8, 1000] M_\odot$ (see Equation (1)). The observed He II/Hγ ratio excludes the steepest IMFs, with particularly strong constraints for a very young system, with stellar ages ⩽1 Myr. In this regime, IMFs with Salpeter-like slopes and with characteristic masses $M_{\rm ch} < 75 M_\odot$ are disfavored at the 1σ level. Since our analysis relies on H and He lines, these IMF constraints remain valid even if C1 is a self-polluted Pop III system: the presence of metals or dust would increase the intrinsic He II/Hγ, reinforcing our conclusions. Furthermore, in our high-density models ($n_{\rm H} = 10^6$ cm^{-3}), the He II/Hγ ratios are mildly affected, thus maintaining our results as valid.

Given these IMF constraints, we infer a total Pop III stellar mass of $2 \cdot 10^4 < M_\star/M_\odot < 6 \cdot 10^5$ to reproduce the observed He II luminosity. Our mass estimates are roughly consistent with predictions from cosmological models and simulations at $z \approx 11$ (e.g., J. Jaacks et al. 2019; E. M. Ventura et al. 2024; R. Hazlett et al. 2025; T. B. Jeong et al. 2026), although on the higher side, which is expected due to the vicinity to a massive galaxy like GN-z11. Assuming a lower maximum mass for Pop III stars would imply even higher stellar masses, in disagreement with theoretical studies. This motivates our choice of employing a Pop III IMF up to $1000 M_\odot$ and further supports our top-heavy IMF scenario. However, strong degeneracies remain between IMF, stellar mass, and age (Figure 3).

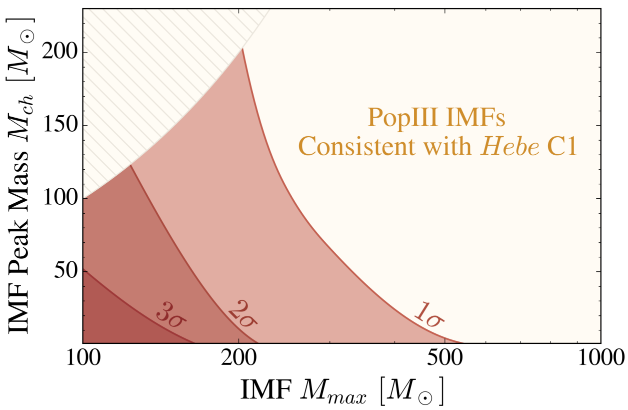

Figure 4. Constraints on the peak ($M_{\rm ch}$) and maximum mass ($M_{\rm max}$) of the Pop III IMF assuming a Salpeter slope, based on the 1σ, 2σ, and 3σ upper limits of He II/Hγ in the C1 component of Hebe (red shaded regions). To maintain the Larson shape of the IMF, the regions with $M_{\rm ch} > M_{\rm max}$ are canceled out.

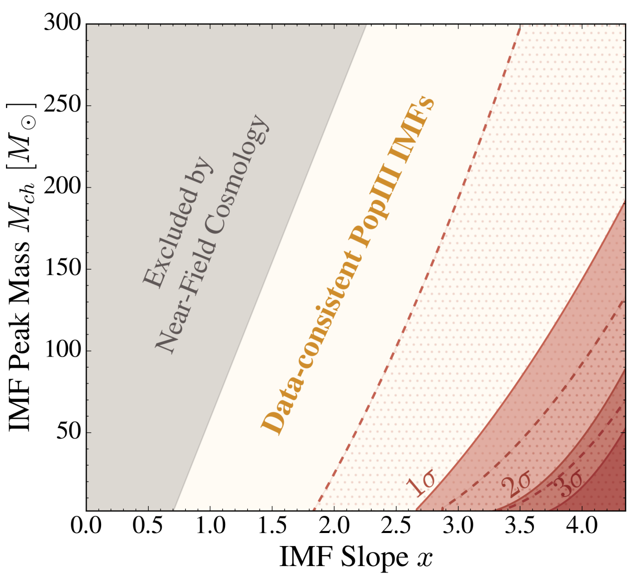

Figure 5. Constraints on Pop III IMF shapes combining our results with near-field cosmology studies (gray area, I. Koutsouridou et al. 2024). Red shaded regions show IMF peaks ($M_{\rm ch}$) and slope (x) excluded by this work based on the 1σ, 2σ, and 3σ upper limits of He II/Hγ in the C1 component of Hebe (left panels in Figure 3). Dotted regions are valid only for ages of 1 Myr.

Extremely top-heavy IMFs, either flat or with a Salpeter slope but with a peak at $M_{\rm ch} \geqslant 140 M_\odot$, i.e., in the mass range of PISNe, are predicted for low stellar masses $\approx$(2–3) $\cdot\, 10^4 M_\odot$. This is particularly intriguing in light of recent results of a putative high-z PISN detection at $z \approx 15$ (A. Ferrara et al. 2026; G. Gandolfi et al. 2026) and the prospect of detecting their chemical signatures in high-z gas clouds (I. Vanni et al. 2024). In this context, C1 may provide direct constraints on the progenitor population of such energetic explosions.

Conversely, steeper Pop III IMFs, such as a Salpeter slope with $M_{\rm ch} = 1 M_\odot$ for the age of 2 Myr, would require stellar masses $\geqslant 10^5 M_\odot$. Such high masses cannot be excluded, as Hebe lies near the luminous galaxy GN-z11 (A. Venditti et al. 2023), whose Lyman–Werner radiation may suppress H_2 cooling in nearby minihalos. However, these masses are higher than typically predicted by simulations that resolve minihalos (e.g., A. Storck et al. 2026). Models with $M_\star < 10^5 M_\odot$ also imply a top-heavy Pop III IMF, as they exclude all IMFs steeper than a Salpeter slope with $M_{\rm ch} < 10\, M_\odot$ (Figure 3). The resulting star formation rates are $(0.018–0.1) M_\odot\ {\rm yr}^{-1}$. Thus, if Pop III stellar masses are limited to the lower values predicted by simulations, our results effectively require top-heavy IMFs.

Figure 5 combines our far-field cosmology Pop III IMF constraints with those from near-field Cosmology studies. The *direct detection* of a pure Pop III system, C1 in Hebe, allows us to exclude the least top-heavy Larson Pop III IMFs: $M_{\rm ch} < ax - 300$, where x is the IMF slope and $a = (111, 88, 80)$ for the 1σ, 2σ, and 3σ lower limits on He II/H$_\gamma$. Conversely, *indirect studies* of the chemical signature of Pop III SNe in Galactic halo stars rule out the flattest ones (I. Koutsouridou et al. 2024). Together, these complementary approaches bracket the Pop III IMF from both ends, providing a data-driven range of viable Pop III IMFs. The most likely IMFs satisfy these conditions: $176x - 331 \leqslant M_{\rm ch} \leqslant 191x - 132$, implying a narrower stellar mass range for C1 in Hebe, $2.5 \cdot 10^4 \lesssim M_\star \lesssim 10^5$. A precise measurement of He II/Hγ would define a direct relation between $M_{\rm ch}$ and the IMF slope, motivating deeper observations of Pop III candidates. Future JWST observations will therefore be critical to transform these constraints into a direct measurement of the Pop III IMF.

Acknowledgments

This project received funding from the ERC Starting grant NEFERTITI H2020/804240 (PI: Salvadori). H.Ü. thanks the Max Planck Society for support through the Lise Meitner Excellence Program. H.Ü. acknowledges funding by the European Union (ERC APEX, 101164796). Views and opinions expressed are, however, those of the authors only and do not necessarily reflect those of the European Union or the European Research Council Executive Agency. Neither the European Union nor the granting authority can be held responsible for them.

Appendix
Impact of a Fully Sampled IMF

To assess the impact of assuming a fully sampled Pop III IMF in our parametric study, we perform 30 test models with the same random sampling technique implemented in NEFERTITI. Consistent with Section 4, we consider Pop III star formation episodes producing total stellar masses of $[10^4, 10^5, 10^6] M_\odot$ and randomly forming stars according to a flat IMF or a Salpeter slope ($x = 2.35$) with $M_{\rm ch} = 10 M_\odot$ (same assumed for Figure 1). We then compute the resulting He II luminosity by summing the contributions of individual Pop III stars, all assumed to have an age of 1 Myr, with fixed $\log U = -1$.

Figure 6 compares the $L_{\rm He\,II}$ resulting from these randomly sampled models with those employed in Section 4, which instead assume fully sampled Pop III IMFs. We also report the predictions for pure Pop III NEFERTITI galaxies of Figure 1, which appear at $M_\star \leqslant 4 \cdot 10^3 M_\odot$.

We find that for large masses of Pop III stars formed ($M_\star \approx 10^6 M_\odot$), the differences in $L_{\rm He\,II}$ are negligible, as the Pop III IMF is effectively fully sampled (e.g., see M. Rossi et al. 2021). Conversely, discrepancies increase toward lower stellar masses, although the $L_{\rm He\,II}$ range spanned by randomly sampled models remains centered around the fully sampled

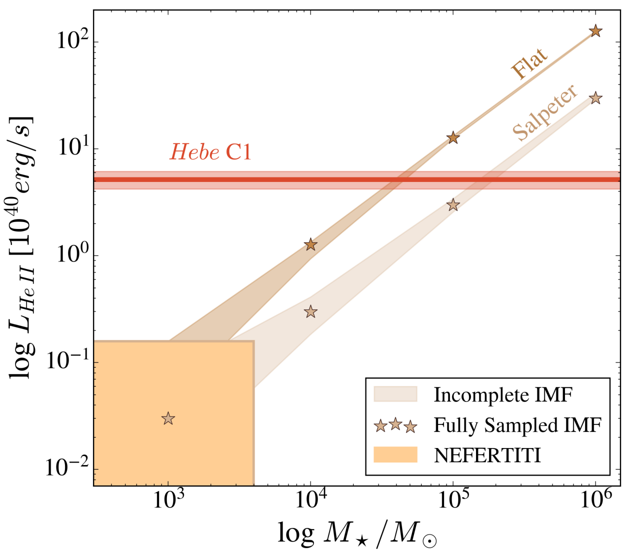

Figure 6. Luminosity of He II λ1640 versus stellar mass for a single burst of Pop III stars with an age of 1 Myr, forming according to Pop III IMF with different slopes: flat (brown) or Salpeter ($x = 2.35$, beige) with $M_{ch} = 10M_\odot$ (see Equation (1)). The stars represent a fully sampled IMF, while the shaded region shows the range obtained by randomly sampling the IMF. The orange region showcases the range of masses and luminosities of pure Pop III NEFERTITI galaxies (IMF slope Salpeter, $M_{ch} = 10M_\odot$). The red line is the measured He II of C1 in Hebe reported by R. Maiolino et al. (2026).

case. For example, at $M_\star = 10^4\,M_\odot$, the fully sampled IMF with Salpeter slope yields $L_{He\,II} = 3 \cdot 10^{39}$ erg s^{-1}, while incomplete sampling gives $L_{He\,II} = (1.8–4.2) \cdot 10^{39}$ erg s^{-1}.

In the lowest-mass regime populated by 80 pure Pop III galaxies from NEFERTITI, the scatter becomes significant, showcasing the importance of stochastic IMF sampling when modeling such very-low-mass systems.

Finally, Figure 6 shows that a Pop III stellar mass of $M_\star = 4 \cdot 10^4\,M_\odot$ ($M_\star = 1.8 \cdot 10^5\,M_\odot$) is required to match the observed He II luminosity of the C1 component in Hebe under a Salpeter IMF (or a flat IMF). This is fully consistent with the results of Section 4 (see in particular, Figure 3, top-right panel).

ORCID iDs

Elka Rusta https://orcid.org/0009-0006-4326-6097
Stefania Salvadori https://orcid.org/0000-0001-7298-2478
Roberto Maiolino https://orcid.org/0000-0002-4985-3819
Viola Gelli https://orcid.org/0000-0001-5487-0392
Ioanna Koutsouridou https://orcid.org/0000-0002-3524-7172
Stefano Carniani https://orcid.org/0000-0002-6719-380X
Hannah Übler https://orcid.org/0000-0003-4891-0794
Alessandro Marconi https://orcid.org/0000-0002-9889-4238
Daniel Schaerer https://orcid.org/0000-0001-7144-7182

References

Bromm, V. 2013, RPPh, 76, 112901
Chatzikos, M., Bianchi, S., Camilloni, F., et al. 2023, RMxAA, 59, 327
Ferland, G. J., Korista, K. T., Verner, D. A., et al. 1998, PASP, 110, 761
Ferrara, A., Carniani, S., Morishita, T., & Stiavelli, M. 2026, arXiv:2601.07374
Gandolfi, G., Rodighiero, G., Castellano, M., et al. 2026, A&A, 706, A364
Hazlett, R., Mead, J., Visbal, E., et al. 2025, arXiv:2510.11629
Inoue, A. K. 2011, MNRAS, 415, 2920
Jaacks, J., Finkelstein, S. L., & Bromm, V. 2019, MNRAS, 488, 2202
Jeong, T. B., Venditti, A., Bromm, V., et al. 2026, arXiv:2603.23209
Klessen, R. S., & Glover, S. C. O. 2023, ARA&A, 61, 65
Koutsouridou, I., Salvadori, S., Skúladóttir, Á., et al. 2023, MNRAS, 525, 190
Koutsouridou, I., Salvadori, S., & Skúladóttir, Á. 2024, ApJL, 962, L26
Koutsouridou, I., Skúladóttir, Á., & Salvadori, S. 2025, A&A, 699, A32
Larson, R. B. 1998, MNRAS, 301, 569
Lecroq, M., Charlot, S., Bressan, A., et al. 2025, A&A, 695, A17
Maiolino, R., Übler, H., Perna, M., et al. 2024, A&A, 687, A67
Maiolino, R., Übler, H., Perna, M., et al. 2026, arXiv:2603.20362
Markov, V., Gallerani, S., Ferrara, A., et al. 2025, NatAs, 9, 458
Morishita, T., Liu, Z., Stiavelli, M., et al. 2025, arXiv:2507.10521
Nakajima, K., & Maiolino, R. 2022, MNRAS, 513, 5134
Nakajima, K., Ouchi, M., Harikane, Y., et al. 2025, arXiv:2506.11846
Nozawa, T., Kozasa, T., Umeda, H., Maeda, K., & Nomoto, K. 2003, ApJ, 598, 785
Oh, S. P., Haiman, Z., & Rees, M. J. 2001, ApJ, 553, 73
Raiter, A., Schaerer, D., & Fosbury, R. A. E. 2010, A&A, 523, A64
Rossi, M., Salvadori, S., & Skúladóttir, Á. 2021, MNRAS, 503, 6026
Rusta, E., Salvadori, S., Gelli, V., Koutsouridou, I., & Marconi, A. 2024, ApJL, 974, L35
Rusta, E., Salvadori, S., Gelli, V., et al. 2025, ApJL, 989, L32
Salvadori, S., Bonifacio, P., Caffau, E., et al. 2019, MNRAS, 487, 4261
Schaerer, D. 2002, A&A, 382, 28
Schaerer, D. 2003, A&A, 397, 527
Schneider, R., Ferrara, A., & Salvaterra, R. 2004, MNRAS, 351, 1379
Storck, A., Katz, H., Devriendt, J., et al. 2026, MNRAS, 548, stag529
Sun, F., Eisenstein, D. J., D'Eugenio, F., et al. 2026, arXiv:2601.15961
Tumlinson, J., & Shull, J. M. 2000, ApJL, 528, L65
Übler, H., Maiolino, R., Pérez-González, P. G., et al. 2026, arXiv:2603.20360
Vanni, I., Salvadori, S., D'Odorico, V., Becker, G. D., & Cupani, G. 2024, ApJL, 967, L22
Vanzella, E., Loiacono, F., Bergamini, P., et al. 2023, A&A, 678, A173
Vanzella, E., Messa, M., Zanella, A., et al. 2026, A&A, 705, L12
Venditti, A., Graziani, L., Schneider, R., et al. 2023, MNRAS, 522, 3809
Ventura, E. M., Qin, Y., Balu, S., & Wyithe, J. S. B. 2024, MNRAS, 529, 628
Zackrisson, E., Rydberg, C.-E., Schaerer, D., Östlin, G., & Tuli, M. 2011, ApJ, 740, 13